2.3 Fundamental Principles and Techniques of Landscape Evolution Modeling

JD Pelletier, University of Arizona, Tucson, AZ, USA

Glossary

Detachment-limited conditions A condition under which the rate of erosion by overland or open-channel flow is related to a detachment rate and no deposition occurs.

Explicit numerical methods Numerical methods in which the value of the quantity being solved for is calculated using variables of the system evaluated at the previous time step only.

Implicit numerical methods Numerical methods in which the value of the quantity being solved for is calculated using variables of the system evaluated at both the current and previous time steps.

Newton's method An iterative method for finding successively better approximations to the solution of a general (e.g., nonlinear) function, using the value of that function and its derivative.

Soil production function A function that quantifies the relationship between the rate of bedrock conversion into regolith/soil and the thickness of soil at that point on the landscape.

Transport-limited conditions A condition under which the rate of erosion or deposition is related to the gradient (in two dimensional (2D)) or divergence (in 3D) of the unit sediment flux.

Abstract

Numerical modeling has become an important method for studying landscape evolution, complementing field- and lab-based techniques such as geologic mapping and geochronology. This chapter describes several techniques used to discretize and solve the most fundamental partial differential equations that arise in landscape evolution. Although landscape evolution modeling encompasses all process zones (hillslope, fluvial, aeolian, glacial, and coastal), this chapter draws primarily from examples in hillslope and fluvial systems. The numerical techniques useful for simulating transport- and detachment-limited landscapes, including alternating direction implicit and upwind differencing methods, as well as root-finding techniques such as Newton's method that are useful for solving nonlinear equations, are emphasized. The chapter also reviews some of the challenges associated with sub-grid-scale processes (e.g., modeling erosion in channels that are not resolved in cross section) and combining different types of processes within numerical models.

2.3.1 Fundamental Processes and Equations

Landscapes evolve in response to tectonic uplift, the weathering of bedrock into regolith, and the transport of sediment by the shear forces of liquid water, wind, and ice. This introductory section describes some of the key processes and equations of hillslope and fluvial geomorphology. Subsequent sections describe specific methods for solving each type of equation. Although this chapter focuses on hillslope and fluvial processes, many of the techniques are suitable for modeling other process types.

2.3.1.1 Conservation of Mass and Overland/Open-Channel Flow

Perhaps the most fundamental equation in landscape evolution is conservation of mass:

$$\frac{\partial z}{\partial t} = -\nabla \cdot \mathbf{q} \qquad [1]$$

Pelletier, J.D., 2013. Fundamental principles and techniques of landscape evolution modeling. In: Shroder, J. (Editor in Chief), Baas, A.C.W. (Ed.), Treatise on Geomorphology. Academic Press, San Diego, CA, vol. 2, Quantitative Modeling of Geomorphology, pp. 29–43.

where z is the local height or thickness of some quantity, t the time, and $\mathbf{q}$ the unit volumetric flux (i.e., the volumetric flux per unit width of flow, expressed in units of length^2 time^{-1}). Equation [1] states that the rate of increase or decrease in some conserved quantity (e.g., depth of water or thickness of sediment) is equal to the negative of the divergence of the volumetric unit flux of that quantity. Equation [1] must be combined with an equation that relates the flux of the conserved quantity to its controlling variables (e.g., flow depth, slope, and bed drag). Flux equations in geomorphology are almost always empirically based, owing to the difficulty of quantifying the turbulent flow of water and sediment in Earth's near-surface environment. For example, the velocity of water in overland or open-channel flow is often assumed to be a function of the hydraulic radius R, the water-surface slope S, and an empirical coefficient, n, used to quantify the drag exerted on the flow by the bed. Manning's equation is one such relationship:

$$v = \frac{R^{2/3} S^{1/2}}{n} \qquad [2]$$

Equations [1] (modified so that h, not z, is the thickness of the conserved quantity) and [2] can be combined to form a single equation for the flow depth h, assuming that the hydraulic radius can be approximated by the flow depth:

$$\frac{\partial h}{\partial t} = -\nabla \cdot \left(\frac{h^{2/3} \left| \nabla z + \nabla h \right|^{1/2} \hat{\mathbf{s}}}{n} \right) \qquad [3]$$

where z is the bed elevation and $\hat{\mathbf{s}}$ the unit vector in the direction of the slope aspect. Equation [3] can be solved for the flow depth, $h_{i,j}$, at every pixel of a raster grid by discretizing the flux term as

$$q_{x_{i+}1/2j} = -\frac{(h_{i+1,j} + h_{i+1,j})^{5/3}}{\Delta x (n_{i+1,j} + n_{i,j})} \left| z_{i+1,j} - z_{i,j} + h_{i+1,j} - h_{i,j} \right|^{1/2} \times sgn(z_{i+1,j} - z_{i,j} + h_{i+1,j} - h_{i,j}) \qquad [4]$$

for the x component, where Δx is the pixel width in the x direction, and

$$q_{y_{i,j+1/2}} = -\frac{(h_{i,j+1} + h_{i,j-1})^{5/3}}{\Delta y (n_{i,j+1} + n_{i,j-1})} \left| z_{i,j+1} - z_{i,j} + h_{i,j+1} - h_{i,j} \right|^{1/2} \times \mathrm{sgn}(z_{i,j+1} - z_{i,j} + h_{i,j+1} - h_{i,j}) \qquad [5]$$

for the y component, where Δy is the pixel width in the y direction. On the right side of Equations [4] and [5], all of the variables refer to values of flow depth, elevation, and roughness at a pixel indexed by (i, j) and their immediate neighbors in the x and y directions. On the left-hand side, the values of flux are indexed at half grid points. This type of indexing is required because fluxes are not defined at a grid point but rather as the material flowing between two grid points. The sums of flow depth and roughness in the numerator and denominator, respectively, appear because the flow depth needed for the calculation of flux is the average of the flow depth between two grid points associated with the flux, not the value at either grid point. The discretization of conservation of mass is given by

$$h_{i,j}(t + \Delta t) = h_{i,j}(t) - \frac{\Delta t}{\Delta x} \left(q_{x_{i+1/2,j}} - q_{x_{i-1/2,j}} \right) - \frac{\Delta t}{\Delta y} \left(q_{y_{i,j+1/2}} - q_{y_{i,j-1/2}} \right) \qquad [6]$$

Source (e.g., rainfall) and sink (e.g., infiltration) terms can be added to Equations [5] and [6] depending on the application. Equation [6] is an explicit method; alternative approaches are discussed in the Section 2.3.2.

As a simplification, many landform evolution models use contributing area or unit contributing area (i.e., the contributing area per unit width of flow) as a proxy for discharge or unit discharge, respectively. Contributing area is calculated using one of several raster-based flow-routing methods. The three most commonly used flow-routing methods are D8 (O'Callaghan and Mark, 1984), multiple flow direction (MFD) (Freeman, 1991; Quinn et al., 1991), and D∞ (Tarboton, 1997). The D8 method routes flow from each pixel toward the neighboring pixel (including diagonals) that represents the steepest descent. D8 has the widely recognized problem that flow pathways are unrealistically restricted to multiples of 45°. The MFD and D∞ methods were designed to avoid this problem, that is, they provide more flexibility by allowing flow to be partitioned among multiple downslope neighbors. The MFD method works by partitioning flow between each pixel and its downslope neighboring pixels by an amount related to the slope in the direction of each downslope neighbor. The D∞ method partitions flow between two adjacent neighboring pixels whose triangular facet (formed by intersection with the center pixel) represents the steepest descent. The MFD method works best in divergent topography while the D∞ method works best in planar or convergent topography based on benchmark calculations of drainage in idealized topography (Tarboton, 1997). Care must be taken when using these methods to compute unit contributing area in order to minimize grid-resolution effects. This point is further addressed later in the chapter.

2.3.1.2 Soil Production and Colluvial Transport on Hillslopes

The rate-limiting process of landscape erosion is the weathering of bedrock into regolith and the transport of that regolith from hillslopes and into channels. Upland (soil over bedrock) hillslopes are comprised of a system of two interacting surfaces: the topographic surface, with elevations given by z, and the underlying weathering front, given by b (**Figure 1**). The difference between these two surfaces is the soil or regolith thickness, denoted as h in this section. The topographic and weathering-front surfaces are strongly coupled because the shape of the topography controls erosion and deposition, which, in turn, controls the values of h (Furbish and Fagherazzi, 2001). The values of h, in turn, control bedrock weathering/soil production rates. This two-way feedback can be quantified as

$$z = b + h \qquad [7]$$

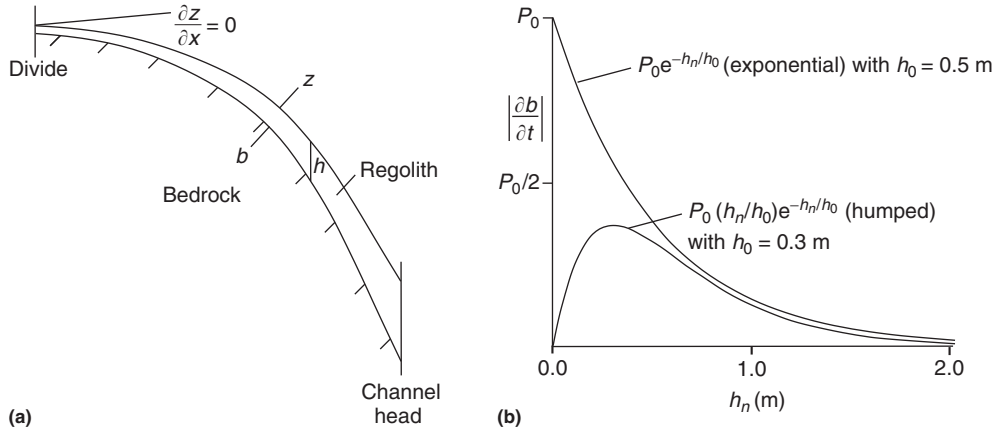

Figure 1 (a) Schematic diagram of a hillslope profile from divide to channel head. (b) Models for the relationship between soil production rate and soil thickness, illustrating the exponential model of Heimsath, A.M., Dietrich, W.E., Nishiizumi, K., Finkel, R.C., 1997. The soil production function and landscape equilibrium. Nature 388, 358–361, with permission from Nature, and an alternative humped model based upon a particular form of the function proposed by Furbish, D.J., Fagherazzi, S., 2001. Stability of creeping soil and implications for hillslope evolution. Water Resources Research 37, 2607–2618, with permission from AGU.

$$\frac{\partial b}{\partial t} = U - \frac{P}{\cos\theta} \quad [8]$$

$$\frac{\partial h}{\partial t} = \frac{\rho_b}{\rho_s}\frac{P}{\cos\theta} - E \quad [9]$$

where ρ_b is the bedrock density, ρ_s the bulk sediment density, P the rate of bedrock recession normal to the surface, θ the slope angle, U the rock uplift rate, and E the erosion rate (Heimsath et al., 1997, 2001). Cosmogenic radionuclide studies indicate that the rate of bedrock recession or weathering normal to the surface decays exponentially with the thickness of overlying regolith measured normal to the surface, $h \cos\theta$:

$$P = P_0 e^{-h\cos\theta/h_0} \quad [10]$$

where P_0 is the bare-bedrock recession rate and h_0 a constant equal to approximately 0.5 m based on cosmogenic radionuclide studies.

Equation [10] states that bedrock lowering is a maximum for bare-bedrock hillslopes and decreases exponentially with increasing regolith thickness. Conceptually, the exponential relationship is a consequence of the buffering effect that regolith has on underlying bedrock, protecting it from diurnal temperature changes and the infiltrating runoff that drive physical and chemical weathering. The exponential soil production function may not capture the full complexity of soil production, however. As soil thickness decreases below a critical value, the landscape may be unable to store enough water to promote weathering or support plant life. Plants act as weathering agents (e.g., root growth can fracture rock and canopy cover can decrease evaporation). As such, in some arid and semi-arid environments, weathering rates may increase with increasing soil thickness for thin soils, activities inconsistent with the exponential model. As such, a humped or bell-shaped relationship of soil production to soil thickness (**Figure 1(b)**) may be more accurate than an exponential relationship (e.g., Ahnert, 1977; Cox, 1980). Recent cosmogenic radionuclide data from granitic landscapes in Australia provide preliminary support for a humped production model (Heimsath et al., 2005).

Erosion on hillslopes occurs by colluvial (e.g., creep and bioturbation) processes and flowing water (e.g., slope/rill wash). The relative importance of these processes varies with distance from the divide, with colluvial processes dominating portions of hillslopes close to divides and slope/rill wash becoming more important near the valley head. The simplest model for erosion by colluvial processes is the diffusion model, first proposed by Culling (1960, 1963). The applicability of the diffusion equation has two requirements: (1) the unit sediment flux must be proportional to slope, that is,

$$\mathbf{q} = -\kappa\nabla z \quad [11]$$

where κ is the diffusivity (units of length^2 time^{-1}), and (2) conservation of mass. Combining Equations [1] and [9] yields the diffusion equation:

$$\frac{\partial z}{\partial t} = \kappa\nabla^2 z \quad [12]$$

The erosion rate E, as defined in Equation [9], is equal to the negative of the value calculated in Equation [12], that is, erosion is defined to be positive if the change in land surface elevation is negative.

To get a better sense for how erosion/deposition is related to topographic curvature on soil-mantled hillslopes, consider a small segment of a hillslope profile (e.g., the section between x_3 and x_4 in **Figure 2**). If more sediment enters the segment from upslope rather than leaving the segment downslope, the hillslope segment must store the difference, resulting in an increase in the average elevation. Conversely, if more sediment leaves the segment downslope rather than entering the segment upslope (as in the section between x_1 and x_2), there is

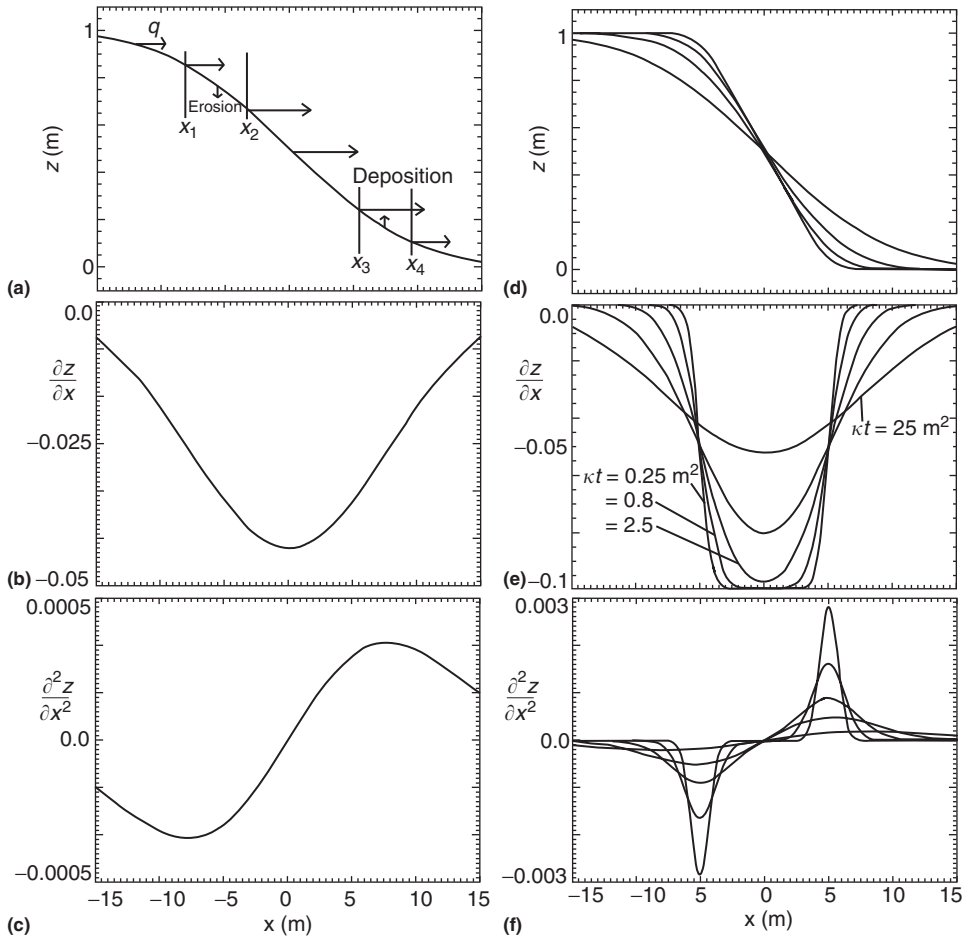

Figure 2 Evolution of a topographic scarp, illustrating (a) elevation, (b) slope, and (c) curvature. In (a), arrows of varying length represent the sediment flux at each point. In the diffusion model, the flux is proportional to the local slope, and the resulting raising or lowering rate of the surface is proportional to the change in flux per unit length, which, in turn, is proportional to the curvature. (d)–(f) Graphs of elevation, slope, and curvature for 5 times following scarp offset ($\kappa t = 0.25$, 0.8, 2.5, 8, and 25 m^2). Modified with permission from Pelletier, J.D., 2008. Quantitative Modeling of Earth Surface Processes. Cambridge University Press, Cambridge.

a net loss of sediment and the elevation must decrease. **Figure 2(a)** illustrates a hypothetical fault scarp 2-m high and 10-m wide after some erosion has taken place. **Figures 2(b)** and **2(c)** illustrate the gradient and curvature of the scarp, respectively. The diffusion equation states that the sediment flux $\mathbf{q}$ at any point along a hillslope is proportional to the hillslope gradient (i.e., **Figure 2(b)**). The magnitude of the flux is illustrated in **Figure 2(a)** at several points along the profile using arrows of different lengths. At the top of the scarp, the flux increases from left to right, indicating that more material is moving out of the section than is being transported into it from upslope. This results in erosion along the top of the scarp where the change in gradient along the profile (i.e., the curvature) is negative. Conversely, flux decreases from left to right at the bottom of the scarp, indicating that more material is moving into that segment than out of it. The result is an increase in surface elevation (i.e., deposition) along the base of the scarp where curvature is positive. The rate of erosion or deposition varies with time according to the magnitude of curvature. Over time, the rate of erosion and deposition decreases, and the widths of the top and bottom of the scarps where erosion and deposition occur increase (**Figure 2(f)**).

Evidence suggests that the diffusion model of hillslope evolution has limited applicability (e.g., Roering et al., 1999; Gabet, 2000; Heimsath et al., 2005). In steep landscapes, the rate of colluvial transport increases nonlinearly with slope as the angle of stability is approached:

$$\mathbf{q} = -\frac{\kappa \nabla z}{1 - (|\nabla z|/S_c)^2} \qquad [13]$$

where S_c is the gradient of hillslope stability. Steep, planar hillslopes and abrupt, knife-edge drainage divides are a signature of landslide-dominated, nonlinear transport on hillslopes (Roering et al., 1999, 2001; Roering, 2004). In addition to the nonlinear slope dependence of hillslope transport processes, there is abundant evidence that rates of colluvial transport depend on the soil thickness. Equations [9] and [11] predict that sediment flux increases abruptly from zero to a finite value as the soil thickness goes from zero to finite. A more realistic approach assumes that sediment flux is

proportional to the soil thickness normal to the slope, at least for relatively thin soils (e.g., less than a couple of meters):

$$\mathbf{q} = -\frac{\kappa h_n \nabla z}{1 - (|\nabla z|/S_c)^2} \quad [14]$$

where κ now has units of length^1 time^{-1} and h_n is the soil thickness normal to the hillslope (Roering, 2008).

2.3.1.3 Erosion and Deposition by Overland and Open-Channel Flow

Erosion and deposition by overland and open-channel flow can be subdivided into transport-limited (TL) and detachment-limited (DL) conditions. Under TL conditions, the rate of erosion/deposition is related to the gradient (in two dimensional (2D)) or the divergence (in 3D) of the unit sediment flux, as in Equation [1]. In DL conditions, the erosion rate is equal to a detachment rate and no deposition occurs. In alluvial channels, TL conditions often predominate because sediment entrained from the channel bed is usually subject to redeposition further downchannel if the transport capacity of the channel decreases via a decrease in flow depth and/or slope. DL conditions may be a good approximation for the erosion of silt-dominated regolith on a hillslope that is subject to sealing/crusting, because, in such cases, most of the regolith may be transported as wash load once it is detached.

It should be noted that TL conditions for regolith erosion on hillslopes and in low-order valleys have been defined in two different ways in the literature. Both definitions assume that sediment transport occurs as bed-material load and that conservation of mass (Equation [1]) applies. Howard (1994a) employed a strict definition in which TL conditions apply only if the actual sediment flux equals the potential sediment flux, that is, the sediment load expected for a cohesionless substrate with no vegetation. If one adopts the above definition, many empirical equations exist that can be used to model the transport of cohesionless sediment grains by overland/open-channel flow. For example, the sediment transport equation of Wiberg and Smith (1989) computes the dimensionless unit sediment flux as a function of the Shields stress, τ_*:

$$\mathbf{q}_* = 9.64\tau_*(\tau_* - \tau_{c*})^{3/2}\hat{\mathbf{s}} \quad [15]$$

where τ_* is the Shields stress and τ_{c*} the critical Shields stress, a parameter that is not constant but varies only slightly as functions of grain size and flow conditions around a representative value of 0.05. The Shields stress is defined, for steady flow conditions, as

$$\tau_* = \frac{hS}{\sqrt{\frac{\rho_s - \rho_w}{\rho_w} D}} \quad [16]$$

where h is the flow depth, S the local slope gradient, ρ_s the density of sediment grains, ρ_w the density of water, and D the mean grain diameter. The unit sediment flux is related to the dimensionless unit sediment flux as

$$\mathbf{q} = \sqrt{\frac{\rho_s - \rho_w}{\rho_w} gDD}\,\mathbf{q}_* \quad [17]$$

Equations [15]–[17] (and similar empirical equations for bedload transport analogous to Equation [15]) can be used to calculate the unit sediment flux by flowing water under steady flow conditions. By combining Equation [17] with conservation of mass (Equation [1]), the evolution of an alluvial channel bed can be modeled over the course of one or more flood events.Adopting the strict definition for TL conditions, that is, that the actual sediment flux equals the potential sediment flux, Howard (1994a) concluded that "erosion by overland flow and ephemeral filling on steep, vegetated slopes is nearly always detachment limited owing to the protection offered by the leaves, stems, and roots … rills and steep washes on badland slopes are generally also detachment-limited owing to the shale or regolith cohesion." Vegetation cover and soil cohesion certainly control a landscape's resistance to fluvial and slope-wash erosion but, whether or not sediment, once detached, is transported primarily as wash load or bed-material load, and hence, whether DL or TL conditions apply, is a separate issue from whether the actual sediment flux equals the potential sediment flux. A less strict definition of TL conditions assumes that sediment flux is proportional to a power function of drainage area (a proxy for discharge) and slope, minus an entrainment threshold, that is,

$$\begin{aligned} \mathbf{q} &= k(A^{m_t} S^{n_t} - \theta_{ct})\hat{\mathbf{s}} \quad \text{if} \quad A^{m_t} S^{n_t} > \theta_{ct} \\ &= 0 \qquad\qquad\qquad\quad \text{if} \quad A^{m_t} S^{n_t} \le \theta_{ct} \end{aligned} \quad [18]$$

where k is a transport coefficient dependent on climate, grain size, and substrate erodibility, m_t and n_t the dimensionless coefficients, θ_{ct} an entrainment threshold below which no transport takes place, and $\hat{\mathbf{s}}$ the unit vector in the direction of the slope aspect. Whether erosion or deposition occurs locally depends on the sign of the divergence of the unit sediment flux.

DL landscape evolution models assume that the rate of fluvial or slope-wash erosion of regolith is proportional to a power function of drainage area and along-channel slope, minus a detachment threshold, that is, the stream-power mode

$$\begin{aligned} \frac{\partial z}{\partial t} &= -K(A^{m_d} S^{n_d} - \theta_{cd}) \quad \text{if} \quad A^{m_d} S^{n_d} > \theta_{cd} \\ &= 0 \qquad\qquad\qquad\quad \text{if} \quad A^{m_d} S^{n_d} \le \theta_{cd} \end{aligned} \quad [19]$$

where K is an erodibility coefficient dependent on climate and substrate erodibility, m_d and n_d the dimensionless coefficients, and θ_{cd} the detachment threshold below which no erosion takes place (Howard, 1994b). In order for Equation [1] to apply, sediment, once detached, must be transported out of the domain in which DL conditions apply without deposition, that is, sediment must be transported primarily as wash load.

The landform evolution models of Smith and Bretherton (1972), Willgoose et al. (1991), Tarboton et al. (1992), Tucker and Bras (1998), Istanbulluoglu et al. (2003), and Simpson and Schlunegger (2003) treat regolith erosion as purely transport

limited, whereas those of Howard (1994b), Moglen and Bras (1995), and Perron et al. (2008, 2009) treat regolith erosion as purely detachment limited. As bed-material load and wash-load sediment transport occur in nearly all landscapes, TL and DL conditions are not mutually exclusive and, in fact, can be expected to occur concurrently in most landscapes. This fact has long been recognized by the soil erosion community (Smith et al., 2010) but, as indicated by the above references, it has been common in the literature on landscape evolution modeling to assume that either DL or TL conditions apply. Recent landscape evolution models of Willgoose (2005), Coulthard et al. (2007), and Wainwright et al. (2008a, 2008b, 2008c), however, do include both DL and TL conditions via a grain-size-dependent approach based on transport distance.

2.3.2 Solution Methods

2.3.2.1 Methods for Diffusive Equations

To solve partial differential equations such as those described above numerically, we must discretize each equation in space and time. The diffusion equation, because of its simplicity, is a particularly useful example for discretization. A standard discretization of the 2D diffusion equation, assuming that $\Delta x = \Delta y$ for simplicity, is given by

$$z_{i,j}^{n+1} = z_{i,j}^{n} + \frac{\kappa \Delta t}{(\Delta x)^2}\left(z_{i+1,j}^{n} + z_{i-1,j}^{n} + z_{i,j+1}^{n} + z_{i,j-1}^{n} - 4z_{i,j}^{n}\right) \quad [20]$$

which is known as the forward time centered space (FTCS) method because the spatial derivatives (i.e., the curvature) are calculated using (i, j) as the center point and because the values at the new time step, $t + \Delta t$ (indexed as $n + 1$), are calculated using just the old values from time t (indexed as n). The FTCS method is useful for solving the diffusion equation on small grids. This scheme is numerically stable provided that the time step is less than or equal to $(\Delta x)^2/(2\kappa)$. Equation [20] is also known as an explicit scheme because the value of each grid point is an explicit function of the grid-point values at the previous time step.

The FTCS method starts with a prescribed initial value for $z_{i,j}$ everywhere on the grid. In addition to the initial condition, boundary conditions on the value of z or its first derivative must also be specified at boundaries of the grid. These boundary conditions may be constant or may vary as a function of time. Equation [20] is then applied to every grid point during each time step of the model. The boundary conditions are then applied (forcing the value of z on the boundaries to be equal to a prescribed value or a prescribed difference from their neighboring values, depending on whether the boundary conditions are fixed z or a fixed derivative of z, respectively) during each time step once all of the interior points have been updated. **Figure 3** illustrates the evolution of diffusive hillslopes responding to instantaneous base-level drop along a series of gullies, for several different times following base-level drop. These results were obtained with the FTCS method.

The FTCS method is generally not useful for large grids because very small step sizes must be taken in order to maintain stability. An alternative approach to FTCS is to write Equation [20] using the new values (those at time step $n + 1$) on the right-hand side of the equation:

$$z_{i,j}^{n+1} = z_{i,j}^{n} + \frac{\kappa \Delta t}{(\Delta x)^2}\left(z_{i+1,j}^{n+1} + z_{i-1,j}^{n+1} + z_{i,j+1}^{n+1} + z_{i,j-1}^{n+1} - 4z_{i,j}^{n+1}\right) \quad [21]$$

which is a matrix equation in which the values of z at all points of the grid are updated simultaneously. Equation [21] is known as the backward Euler method. It is also called an implicit method because the values at the new time step appear on both sides of the equation. The order of the matrix in Equation [21] is equal to the number of grid points, hence solving Equation [21] typically requires inverting a very large matrix.

The accuracy of Equation [21] and its ease of use can both be improved using the Alternating direction implicit (ADI) method. In this method, the 2D problem of Equation [21] is divided into a series of 1D problems, that is, first all of the rows are solved for and then all of the columns:

$$\begin{aligned} z_{i,j}^{n+1/2} &= z_{i,j}^{n} + \frac{\kappa \Delta t}{2(\Delta x)^2}\left(z_{i+1,j}^{n+1/2} + z_{i-1,j}^{n+1/2} - 2z_{i,j}^{n+1/2} + z_{i,j+1}^{n} + z_{i,j-1}^{n} - 2z_{i,j}^{n}\right) \\ z_{i,j}^{n+1} &= z_{i,j}^{n+1/2} + \frac{\kappa \Delta t}{2(\Delta x)^2}\left(z_{i+1,j}^{n+1/2} + z_{i-1,j}^{n+1/2} - 2z_{i,j}^{n+1/2} + z_{i,j+1}^{n+1} + z_{i,j-1}^{n+1} - 2z_{i,j}^{n+1}\right) \end{aligned} \quad [22]$$

This approach has two advantages. First, it is centered in time (i.e., the curvature term on the right side of the equation is an average of the curvature values at the beginning and end of the time step); therefore, it is more accurate than the backward Euler method of Equation [21], which uses only the curvature from the end of the time step. Second, by breaking up the problem into a series of 1D diffusion problems (i.e., solving rows and columns along the x and then along y directions separately), the matrix that has to be solved is both smaller and has a simpler, tri-diagonal form.

Implicit methods are far more stable than explicit methods. In fact, the implicit method is stable for any time step. The accuracy of the solution, however, still depends on the time step. In practice, it is useful to run two versions of the same implicit simulation with time steps that differ by a factor of 2. The difference between the two solutions provides an estimate of the accuracy of the results for the larger time step. The ADI and FTCS methods are useful for many flux-conservative equations (i.e., those in which conservation of mass applies), not just diffusion.

2.3.2.2 Methods for Advective Equations

Solving stream-power or DL equations requires a fundamentally different approach than solving TL or diffusive equations. The stream-power model is an example of an advection equation, which in a simple but general form is given by

$$\frac{\partial z}{\partial t} = c\frac{\partial z}{\partial x} \quad [23]$$

where c is a coefficient that can be either constant or a function of space and/or time. Advection equations involve the lateral translation of some quantity. The coefficient c in

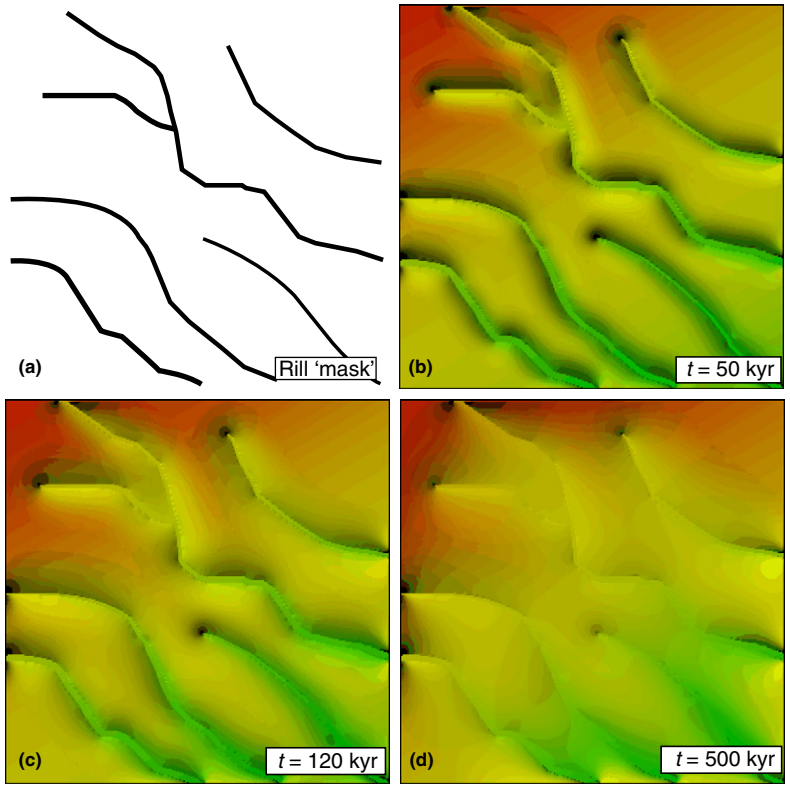

Figure 3 Solution to the diffusion equation with $\kappa = 1\ \mathrm{m^2\ kyr^{-1}}$ in the neighborhood of a series of gullies (shown in (a)) kept at constant base level and a model domain of 0.01 $\mathrm{km^2}$. This model represents the evolution of an alluvial-fan terrace abruptly entrenched at time $t = 0$. After (b) 50 kyr, diffusional rounding of the terrace near gullies has penetrated $\approx\sqrt{\kappa t}$ or 7 m into the terrace tread and planar terrace treads are still widely preserved. After (c) 120 kyr, approximately 11 m of rounding has taken place. Finally, after (d) 500 kyr, erosional processes have removed all planar terrace remnants and a rolling ridge-and-ravine topography remains. Modified with permission from Pelletier, J.D., 2008. Quantitative Modeling of Earth Surface Processes. Cambridge University Press, Cambridge.

Equation [23] has units of length over time and represents the speed at which z is advected laterally. In the context of landform evolution, the advection equation is used to model retreating landforms, including cliffs, banks, and bedrock-channel knickpoints. The stream-power model (Equation [19]) with $m_\mathrm{d} = 1/2$ and $n_\mathrm{d} = 1$ and no detachment threshold, that is,

$$\frac{\partial z}{\partial t} = -KA^{1/2}\left|\frac{\partial z}{\partial x}\right| \qquad [24]$$

where x is the distance from the divide, is simply an advection equation with spatially variable advection coefficient. Conceptually, the stream-power model says that the action of bedrock-channel incision can be quantified by advecting the topography upstream with a local rate proportional to the square root of contributing area.

The FTCS method is inherently unstable when applied to advection problems. However, upwind differencing provides a simple, useful numerical method for advection equations. As applied to Equation [24], upwind differencing means simply that the along-channel slope is always calculated in the direction of steepest descent. More generally, that is, in Equation [23] where c varies in space and/or time, upwind differencing involves calculating the slope along the direction of transport, that is,

$$z_i^{n+1} = z_j^n + \Delta t c_i^n \begin{Bmatrix} z_{i+1}^n - z_i^n & \text{if} & c_i^n > 0 \\ z_i^n - z_{i-1}^n & \text{if} & c_i^n < 0 \end{Bmatrix} \qquad [25]$$

In the FTCS technique, the centered-space gradient is calculated by taking the difference between the value of the grid point to the left (i.e., at $i-1$) and the value to the right (i.e., at $i+1$) of the grid point being updated. This approach is prone to instability because it does not make use of the value at the grid point i itself. As such, the difference $z_{i+1}^n - z_{i-1}^n$ can be small even if the value of z_i^n is wildly different from the values on either side of it. In effect, the FTCS method creates two largely decoupled grids (one with even i and the other with odd i) that drift apart from each other over time. In the upwind method, this problem is corrected by calculating gradients using only one adjacent point. If the flux of material is moving from left to right, then physically it makes sense that the value of z_i^{n+1} should depend on z_{i-1}^n, not on z_{i+1}^n. Conversely, of the flux of material is in the opposite direction, z_i^{n+1} should depend on z_{i+1}^n. The upwind differencing method implements that approach.

Figure 4(a) illustrates the evolution of a knickpoint modeled with Equation [23] using the upwind differencing method. One drawback of the upwind differencing

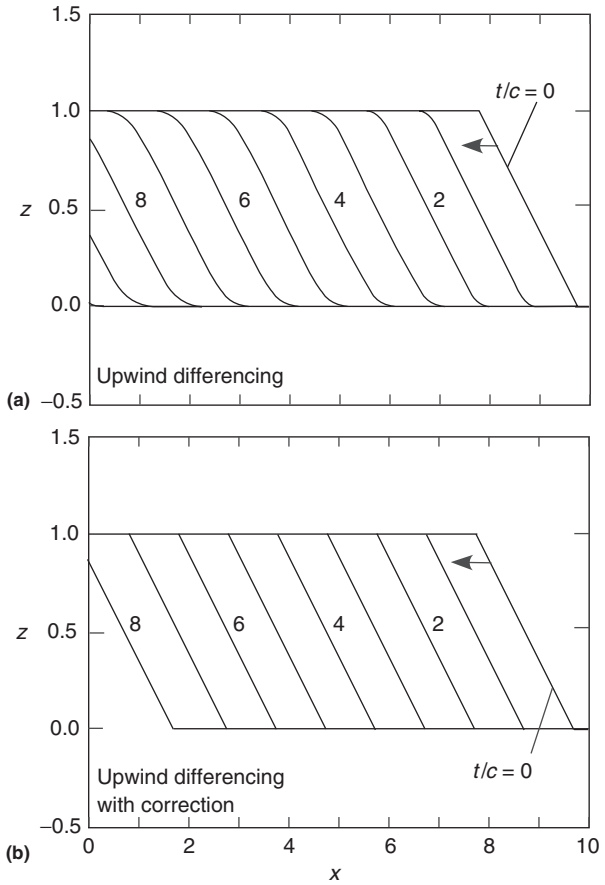

Figure 4 Solution to the advection equation for an initial condition of a hypothetical knickpoint (a) with upwind-differencing and (b) including the Smolarkiewicz correction. Without the correction, the knickpoint in (a) gradually acquires a rounded top and bottom. With the correction, the initial knickpoint shape is preserved almost exactly as it is advected upstream. Modified from Pelletier, J.D., 2008. Quantitative Modeling of Earth Surface Processes. Cambridge University Press, Cambridge.

method is illustrated in this figure: a small amount of numerical diffusion enters into the solution over time. Smolarkiewicz (1984) proposed a correction step that greatly reduces this numerical diffusion. **Figure 4(b)** illustrates the results of the knickpoint simulation with Smolarkiewicz correction. These results are essentially exact: knickpoint retreat at a constant rate with no change in the shape of the knickpoint.

Figure 5 illustrates the behavior of a numerical landform evolution model incorporating stream-power erosion, solved with upwind differencing, for a vertically uplifted, low-relief plateau 200 km in width. Uplift occurs at a constant rate $U = 1$ m kyr^{-1} for the first 1 Myr of the simulation and a value of $K = 3 \times 10^{-4}$ kyr^{-1} was assumed. The contributing area required by Equation [24] is calculated in each time step using the multiple-flow-direction algorithm of Freeman (1991). Isostatic rebound was also included by assuming regional compensation over a prescribed flexural wavelength and averaging the erosion rate over that wavelength (here assumed to be 200 km, the width of the model domain). In the model, uplift initiates a wave of bedrock incision in which channel knickpoints propagate rapidly through the drainage basin. In this model, knickpoints reach the drainage headwaters after 25 Myr and the maximum elevation at that time is nearly 3 km. Following 25 Myr, the range slowly erodes to its base level.

2.3.2.3 Methods for Solving Nonlinear Equations

The introduction presented the fundamental equations for the generation and transport of regolith on hillslopes. The equation for the rate of change of regolith thickness, using the exponential soil production function and the diffusion model for hillslope evolution, is

$$\frac{\partial h}{\partial t} = \frac{\rho_b}{\rho_s}\frac{P_0}{\cos\theta}e^{-h\cos\theta/h_0} + \kappa\nabla^2 z \qquad [26]$$

One application of this model involves solving for the steady-state soil thickness given knowledge of the topography (e.g., from airborne Light Detection and Ranging (LiDAR) data). Setting Equation [26] equal to zero and solving for h gives

$$h = \frac{h_0}{\cos\theta}\ln\left(-\frac{\rho_b}{\rho_s}\frac{P_0}{\kappa\cos\theta}\frac{1}{\nabla^2 z}\right) \qquad [27]$$

Alternatively, if one assumes that sediment flux is depth dependent, that is, that the flux is equal to the product of κ, h cos θ, and slope, then the resulting equation for the steady-state regolith thickness is

$$f(h) = \frac{\rho_b}{\rho_s}\frac{P_0}{\cos\theta}e^{-h\cos\theta/h_0} + \kappa h\cos\theta\nabla^2 z + \kappa\nabla(h\cos\theta)\cdot\nabla z = 0 \qquad [28]$$

which cannot be solved algebraically. Newton's method is a powerful technique for solving nonlinear equations such as this. Given an initial guess for the regolith thickness at a point on the grid (e.g., zero), a better approximation to the solution is given by

$$h_{n+1} = h_n - \frac{f(h_n)}{f'(h_n)} \qquad [29]$$

where h_n is the value of regolith thickness at iteration n in the Newton's method. **Figure 6** illustrates the steady-state soil thicknesses obtained by solving Equation [28] corresponding to a range of values of the nondimensional parameter $(\rho_b/\rho_s)P_0/\kappa$ for a region in the Mojave Desert. These maps were produced using Newton's method. The soil thickness at each value of the grid was solved in descending order of elevation, starting at the highest elevation (where there is no sediment flux from upslope) and moving downhill, using the values of h in the upslope directions in x and y in order to compute the gradient of h in Equation [28] corresponding to each trial value. Based on field measurements of soil thickness, the value $(\rho_b/\rho_s)P_0/\kappa = 0.03$ provides reasonable predictions for soil thickness in this study area based on a comparison with available field data (not shown).

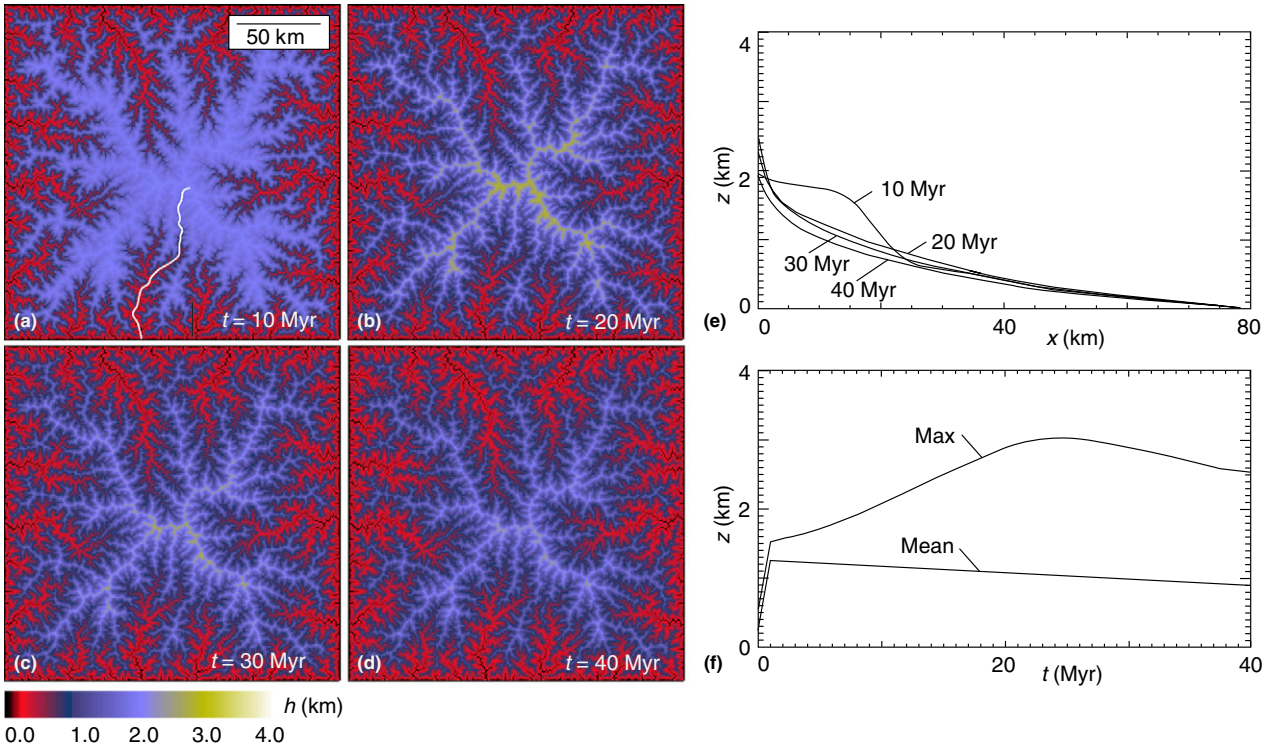

Figure 5 Model results for the stream-power model following 1-km uniform block uplift of an idealized mountain range. In the stream-power model, knickpoints rapidly propagate into the upland surface, limiting the peak elevation to ≈3 km at 25 Myr following uplift.

2.3.2.4 Combining Process Models and Minimizing Grid-Resolution Dependence

This section describes some of the challenges involved in combining process models and minimizing their grid-resolution dependence. In many models, multiple process types (e.g., diffusive and advective processes) coexist in many pixels. How to weigh the relative importance of each process type is often unclear, especially given that any model is necessarily an incomplete (i.e., subsampled) representation of the actual landscape being modeled.

Two alternative approaches have been taken to combining colluvial and fluvial/slope-wash processes in landscape evolution models. Howard (1994b) assumed that the value of z in each pixel represents the average elevation, including both hillslope and channel/valley components. This approach requires the user to prescribe the relative importance of fluvial and hillslope processes in each pixel. Howard (1994b), for example, assumed that each pixel contains one and only one channel; hence, fluvial processes are assumed to act on a subset of the area of each pixel equal to w/δ, where w is a prescribed channel width and δ the pixel width. One problem with this approach is that the density of channels (a property of the natural landscape that must be independent of grid resolution) is forced to be inversely proportional to the pixel width, for example, the channel density doubles as the pixel size is halved. A second problem is that the derivative of z in this approach is not equal to the slope of the fluvial pathway (as required by the stream-power model), but rather is the derivative of some average elevation that includes both hillslope and channel/valley components. An alternative approach advocated by Pelletier (2010) is to treat the value of z in each pixel as the elevation of the dominant fluvial pathway in each pixel. The dominant fluvial pathway acts as the base level of erosion for all the sub-grid-scale topography within the area represented by that pixel. The topography within a grid point adjusts to the elevation of the dominant fluvial pathway; hence, it is only necessary to track the erosion of that point. This alternative approach does not require that the relative dominance of fluvial and colluvial processes in each pixel be prescribed, because only the erosion of the dominant fluvial pathway (which may be a channel, rill, or zone of sheetflow) in each pixel is being tracked by the model. A third approach, used by Pelletier (2008), does not attempt to combine colluvial and fluvial/overland flow processes in individual pixels, but rather assumes that fluvial/overland flow is negligible on hillslopes and that colluvial processes are negligible in valleys. In this approach, a drainage density must be prescribed and only colluvial processes are applied to areas where the product of slope and the square root of contributing area are greater than a threshold value equal to the inverse of the drainage density, as observed empirically by Montgeomery and Dietrich (1988). The drawback of this approach is twofold: (1) it introduces a new parameter into the model, the drainage density, which ultimately must be a function of other variables in the model (e.g., substrate erodibility K and diffusivity κ) and (2) it does not model the coexistence/competition between colluvial and slope-wash/fluvial processes in the vicinity of valley heads.

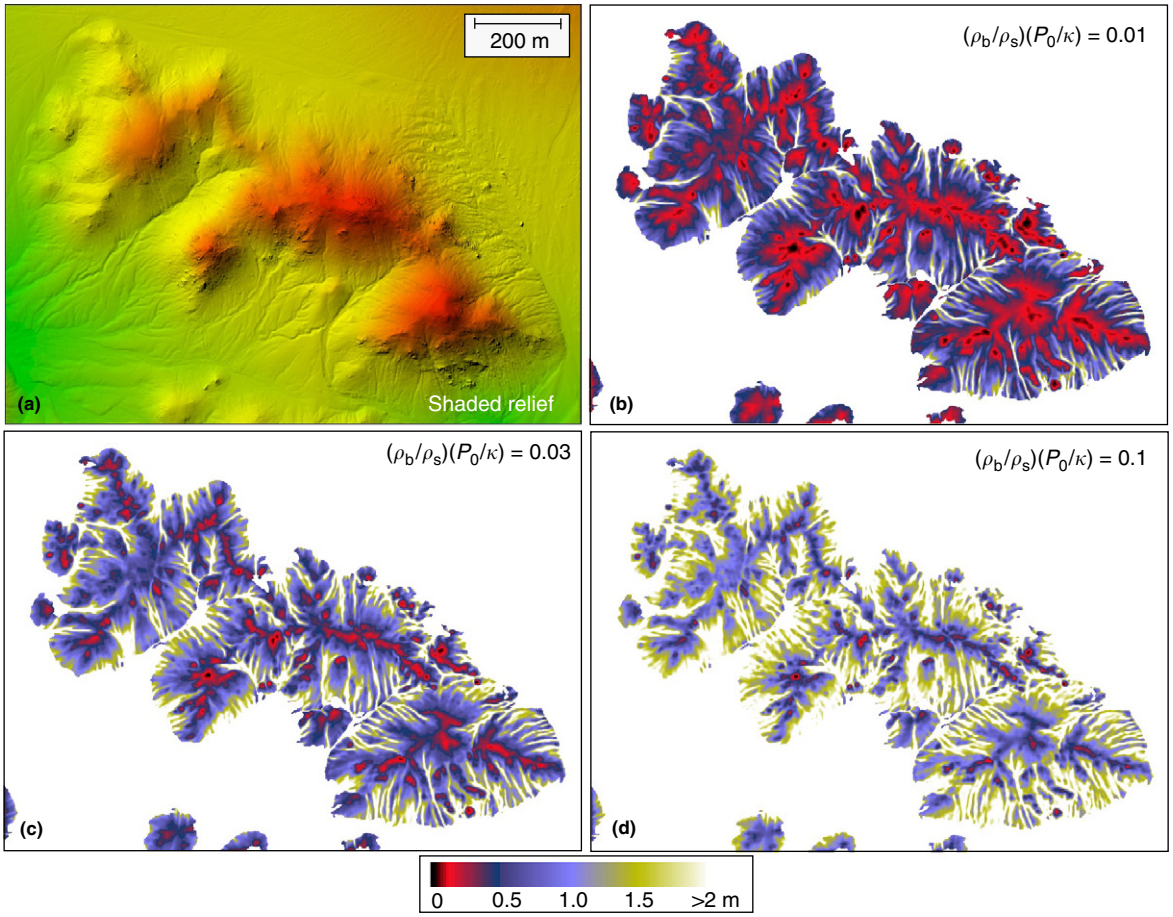

Figure 6 Maps of soil thickness for an upland area in Fort Irwin, California. (a) Shaded-relief image of the area from a 1-m DEM derived from airborne LiDAR. (b)–(d) Soil thickness predicted by the model described in the text for $(\rho_b/\rho_s)(P_0/\kappa) =$ (b) 0.01, (c) 0.03, and (d) 0.1.

To minimize the grid-resolution dependence of landform evolution models that quantify slope-wash and fluvial erosion/deposition using the contributing area, it is also necessary to make some modifications to the existing flow-routing algorithms. The contributing areas computed by existing flow-routing algorithms depend on grid resolution. To minimize this problem, it is necessary to formulate fluvial/slope-wash erosion and transport relationships in terms of the unit contributing area, that is, the contributing area per unit width of flow, rather than the contributing area. Landform evolution models in which fluvial erosion rates are assumed to be a power-law function of unit stream power, for example, should have the form

$$\begin{aligned}\frac{\partial z}{\partial t} &= \frac{\rho_b}{\rho_s}U - K\left(\left(\frac{A}{w}\right)^{p_d} S^{n_d} - \theta_{cd}\right) \quad \text{if} \quad \left(\frac{A}{w}\right)^{p_d} S^{n_d} > \theta_{cd} \\ &= \frac{\rho_b}{\rho_s}U \qquad\qquad\qquad\qquad\quad \text{if} \quad \left(\frac{A}{w}\right)^{p_d} S^{n_d} \le \theta_{cd}\end{aligned} \qquad [30]$$

where w is the width of flow in the dominant fluvial pathway within each pixel and p_d a dimensionless coefficient. It should be noted that the units of K and θ_c differ depending on the value of p_d. Equation [30] also includes a source term, $(\rho_b/\rho_s)U$. The form of that term implicitly assumes that regolith covers the landscape, that is, at the surface, all bedrock has been converted to soil prior to erosion.

In tributary valleys, it is generally a good approximation to assume that the width of the flow is proportional to a power function of the contributing area (a proxy for discharge), that is,

$$w_v = cA^b \qquad [31]$$

where $b \approx 1/2$ and c is a coefficient that varies between drainage basins (Leopold and Maddock, 1953). The w in Equation [31] has a subscript v to indicate that Equation [31] is used to calculate flow width on valleys only. Substituting Equation [31] into Equation [30] and subsuming the coefficient c into K and θ_c yield the familiar form of the stream-power erosion model for regolith-covered landscapes (Equation [19]) where $m_d = p_d - b$. If $p_d = 1$ and $b = 1/2$, for example, $m_d = 1/2$. The formulation based on A/w (i.e., Equation [30]) is more fundamental than the formulation based on A (i.e., Equation [19]) because Equation [30] does not require that the power-law relationship between contributing area and flow width (i.e., Equation [31]) applicable to tributary valleys applies throughout the landscape. On

hillslopes, the width of flow in each pixel is equal to the pixel width, that is, $w_h = \delta$, if flow occurs as sheetflooding. Alternatively, if flow occurs in finely spaced parallel rills, the width of flow within the dominant fluvial pathway is equal to the flow in each rill, that is, $w_h = (w_r/\lambda_r)\delta$, where w_r is the width of flow in each rill and λ_r is the rill spacing.

Figure 7(a) schematically compares the results of flow routing on digital elevation models (DEMs) representing planar and convergent hillslopes. On a planar hillslope, flow is routed in the direction of the slope aspect. The contributing area of each pixel at the slope base is, therefore, equal to $L\delta$, where L is the length of the slope and δ the pixel width. At the outlet of the convergent slope (the point to which all flow is routed in this hypothetical example), the contributing area is equal to L^2. As such, the contributing areas of pixels on planar hillslopes depend on pixel width, whereas the contributing areas of pixels in zones of strongly convergent flow (where all flow is focused into a pathway narrower than a pixel width) do not depend on pixel width. This problem is perhaps best illustrated using specific flow-routing methods in idealized topographic cases. **Figures 7(c)** and **7(d)** illustrate the ratios of contributing area calculated by the MFD and D∞ methods on a synthetic second-order drainage basin (illustrated in **Figure 7(b)**) with pixel width of δ to the contributing area of the same drainage basin bilinearly interpolated to a pixel width of $\delta/2$ (shown here for $\delta = 0.25$ m). In this analysis, the contributing area computed on the interpolated grid is subsampled to the same resolution as the original grid, adopting the maximum value for contributing area within the 2 pixel $\times$ 2 pixel subdomains of the interpolated DEM that represent each pixel in the original DEM. For a flow-routing algorithm to be scale independent, the ratio of the contributing area calculated with pixel width δ to the contributing area of the exact same DEM interpolated to a pixel width of $\delta/2$ and then subsampled back to the original pixel width should be 1 or nearly 1 everywhere on the landscape. The fact that this ratio differs significantly from 1 (i.e., it is close to 2 on most areas of the hillslope (as indicated by the mostly white area) and close to 1 in the pixels that comprise the tributary valley network) indicates that the MFD and D∞ methods are scale dependent when it comes to computing the maximum value of contributing area across different scales of model resolution. This is a general problem for any value of δ and for any landscape that includes hillslopes of variable convergence and/or both hillslopes and valleys.

One can minimize the scale dependence of flow-routing methods using the maps in **Figure 7** as input to a correction step. In this approach, a flow-routing algorithm (e.g., MFD and D∞) is first applied to the landscape to compute contributing area. Then, the flow-routing method is applied to the same landscape bilinearly interpolated to have a pixel width equal to one-half of the original grid, as in the analysis presented in **Figures 7(c)** and **7(d)**. The contributing area computed from the interpolated grid is then subsampled to the same resolution as the original grid, adopting the maximum value for contributing area within the 2 pixel $\times$ 2 pixel subdomains of the interpolated DEM that represent each pixel in the original DEM. The maximum value within each subdomain is chosen because the goal is to quantify the fluvial erosion rate of the dominant fluvial pathway within each pixel. The ratio of these two contributing area maps is then computed and denoted as f. The unit contributing area, a, is

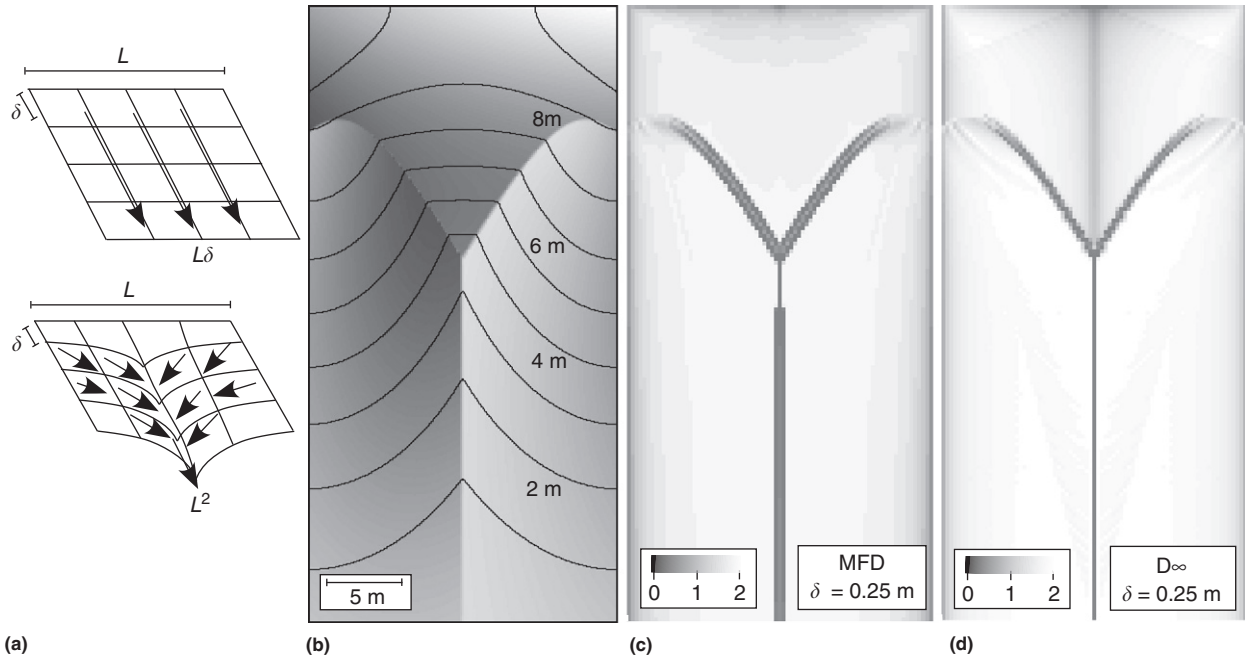

Figure 7 Dependence of flow-routing methods on grid resolution. (a) Schematic illustration of flow in planar (top) and convergent (bottom) hillslopes. On planar hillslopes, contributing area at the slope base is equal to $L\delta$, where δ is the pixel width, whereas in convergent hillslopes it is L^2. (b) Shaded relief and contour map of synthetic second-order drainage basin. (c)–(d) Ratio of contributing area calculated with pixel width δ to the contributing area of the same drainage basin bilinearly interpolated to a pixel width $\delta/2$ (shown here for $\delta = 0.25$ m) for (c) the MFD method and (d) the D∞ method.

then calculated as

$$\begin{aligned} a &= \frac{A}{w_h} \quad \text{if} \quad f \geq 1.2 \\ &= \frac{A}{w_v} \quad \text{if} \quad f < 1.2 \end{aligned} \qquad [32]$$

where w_h is the flow width on hillslopes (i.e., $w_h = \delta$ if flow occurs as sheetflooding and $w_h = (w_r/\lambda_r)\delta$ if flow occurs in parallel rills) and w_v is given by Equation [31]. This approach exploits the fact that the values of f differ on hillslopes (i.e., varying from approximately 1.2 to 2.0 depending on the degree of convergence) and in valleys (i.e., nearly equal to 1) in order to normalize the contributing area by the appropriate value of the width of the flow in each type of pixel (hillslope or valley). Results obtained with the synthetic landscape of **Figure 7(b)** suggest that a cutoff value of 1.2 works best for distinguishing between hillslope and valley pixels, that is, if the cutoff value is set significantly lower than 1.2, portions of first-order valleys are misidentified as hillslopes, whereas if the value is set significantly higher than 1.2, portions of convergent hillslopes are misidentified as valleys.

To combine hillslope diffusion and fluvial erosion within a framework in which z represents the elevation of the dominant fluvial pathway within each pixel, it is also necessary to scale the rate of erosion/deposition from hillslope processes by the ratio δ/w for models with grids sufficiently coarse that channels are not explicitly resolved in cross section (as assumed here). On hillslopes with unconfined flow, the ratio δ/w is 1; hence, the rate of erosion or deposition by hillslope processes is unaffected by this scaling. In valleys, however, the rate of deposition that occurs in the dominant fluvial pathway within each pixel is systematically underpredicted because the fluvial pathway is not resolved in cross section. The cross-sectional curvature is equal to the difference in the gradient of the side slopes adjacent to the dominant fluvial pathway divided by the width of that pathway. In a grid, in which the flow width is narrower than the pixel width, the curvature will, therefore, be underestimated by a factor of δ/w, assuming that the gradients of the side slopes are adequately resolved. As such, it is necessary to scale the curvature values by δ/w to predict the correct deposition rate within the dominant fluvial pathway of each pixel. Integrating colluvial processes in this way into Equation [30] gives

$$\begin{aligned} \frac{\partial z}{\partial t} &= \frac{\rho_b}{\rho_s} U + \frac{\delta}{w}\kappa\nabla^2 z - K(a^{p_d} S^{n_d} - \theta_{cd}) \quad \text{if} \quad a^{p_d} S^{n_d} > \theta_{cd} \\ &= \frac{\rho_b}{\rho_s} U + \frac{\delta}{w}\kappa\nabla^2 z \qquad\qquad\qquad\qquad\quad \text{if} \quad a^{p_d} S^{n_d} \leq \theta_{cd} \end{aligned} \qquad [33]$$

for the DL model, where $a = A/w$, and, for TL model,

where

$$\frac{\partial z}{\partial t} = \frac{\rho_b}{\rho_s} U + \frac{\delta}{w}\kappa\nabla^2 z - \nabla \cdot \mathbf{q} \qquad [34]$$

$$\begin{aligned} \mathbf{q} &= k(a^{p_t} S^{n_t} - \theta_{ct})\hat{\mathbf{s}} \quad \text{if} \quad a^{p_t} S^{n_t} > \theta_{ct} \\ &= 0 \qquad\qquad\qquad\quad \text{if} \quad a^{p_t} S^{n_t} \leq \theta_{ct} \end{aligned} \qquad [35]$$

The models illustrated in **Figures 8** and **9** solve Equation [33] for the DL model and Equations [34] and [35] for the TL model, assuming a gently sloping (1%) initial landscape. Observed slope–area relationships in channels (e.g., $S \propto A^{-b}$ with b in the range of 0.35–0.6) imply that p_d/n_d is in the range of approximately 0.7–1.2 and p_t/n_t is in the range of approximately 1.7–2.2, assuming $w_v \propto A^{1/2}$. Channel gradients are generally observed to be a power-law function of drainage area with an exponent between -0.35 and -0.6 for both DL and TL conditions (e.g., Hack, 1957; Tarboton et al., 1992; Ijjasz-Vasquez and Bras, 1995; Whipple and Tucker, 1999). This implies values for m/n of between approximately 0.35 and 0.6 if DL conditions and steady state are assumed, that is, $m_d = 0.35 - 0.6$ or $p_d = 0.7 - 1.2$ if $n_d = 1$. For steady state to be achieved in the TL model, the unit sediment flux must be proportional to the unit contributing area, implying a value for $\frac{1}{2}(p-1)/n$ of approximately between 0.35 and 0.6 (Tarboton et al., 1992; Istanbulluoglu et al., 2003), that is, $p_t = 1.7 - 2.2$ if $n_t = 1$. The fluvial/slope-wash erosion component of each model is solved for at each time step of the model by calculating S in the downslope direction using a time step that satisfies the Courant stability criterion. The diffusive component of each model is calculated using the ADI technique.

In topographic steady state, landscapes produced with the DL and TL models are qualitatively quite similar, as landscape evolution models produced with DL and TL models over

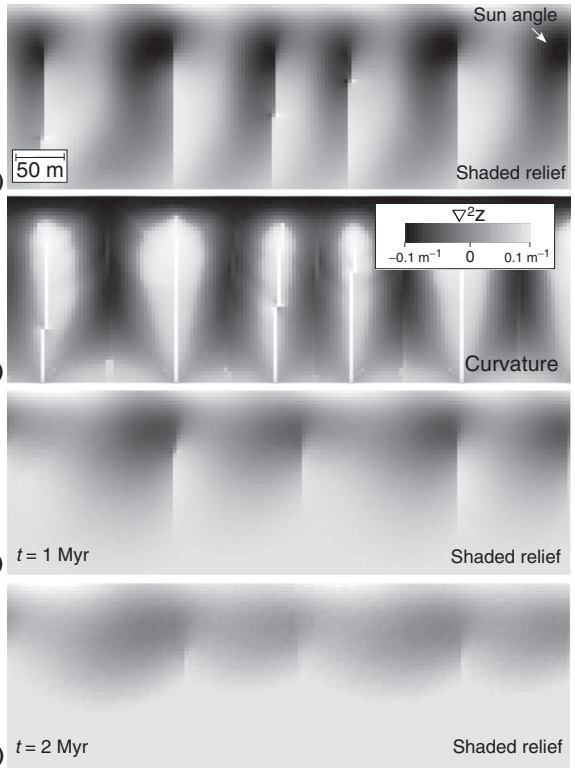

Figure 8 Evolution of a model DL landscape driven to an approximate steady-state condition (shown in (a) and (b)) followed by topographic decay (i.e., uplift rate set to zero) (shown in (c) and (d)). Model parameters are $p_d = 1$, $(\rho_b/\rho_s)U = 0.1$ m kyr^{-1}, $\kappa = 1$ m^2 kyr^{-1}, $K = 0.0005$ kyr^{-1}, $c = 0.01$, $\theta_c = 10$ m, rilled hillslopes with $w_h = 0.1\delta$, and a model domain of 250 m × 750 m. (a), (c), and (d) illustrate topography/elevation, (b) illustrates topographic curvature.

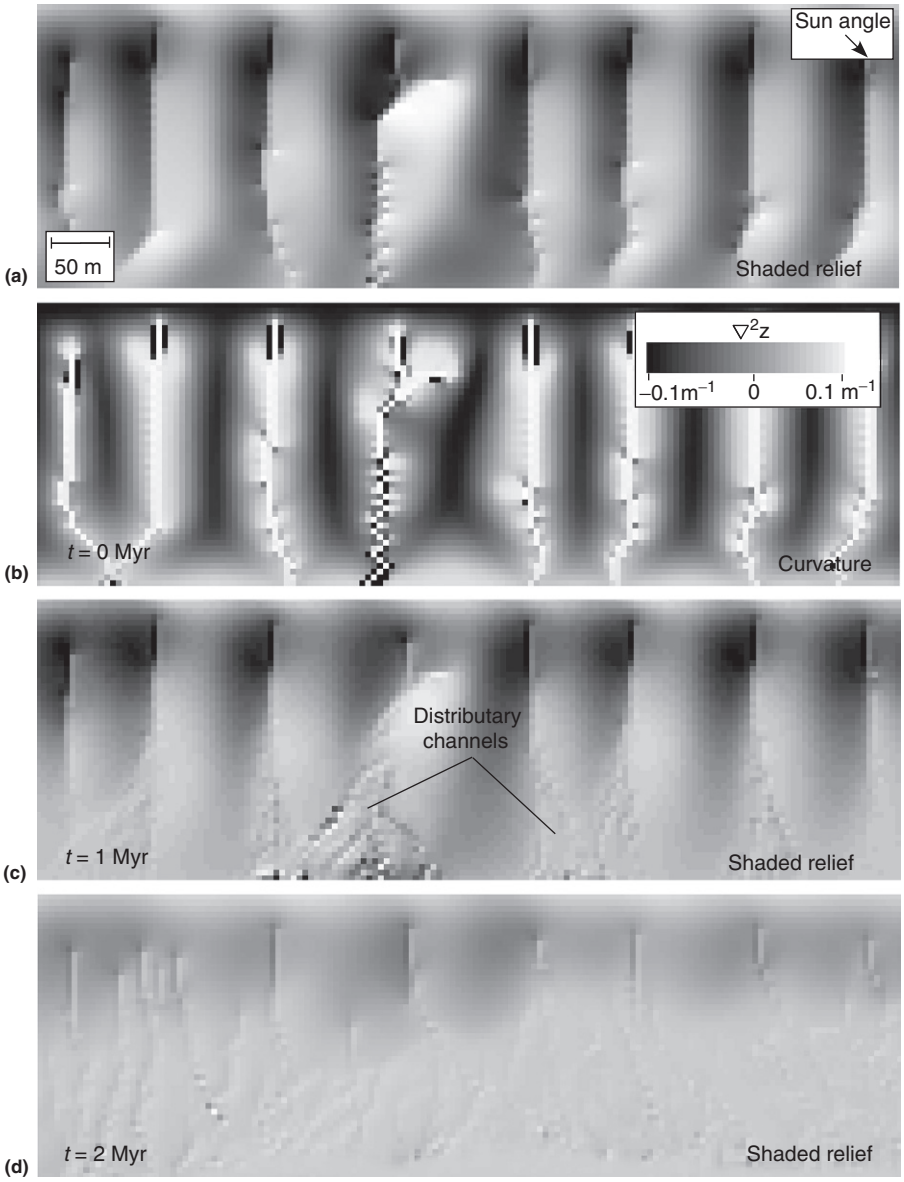

Figure 9 Evolution of a model TL landscape driven to an approximate steady-state condition (shown in (a) and (b)) followed by topographic decay (i.e., uplift rate set to zero) (shown in (c) and (d)). Model parameters are $p_t = 5/3$, $(\rho_b/\rho_s)U = 0.1$ m kyr^{-1}, $\kappa = 1$ m^2 kyr^{-1}, $k = 0.0001$ m$^{2/3}$ kyr^{-1}, $c = 0.01$, and $\theta_c = 1$ m, rilled hillslopes with $w_h = 0.1\delta$, and a model domain of 250 m × 750 m. (a), (c), and (d) illustrate topography/elevation, (b) illustrates topographic curvature.

the past 20 years have illustrated. Indeed, the similarity in landscape form predicted by these two end-member model types is one reason that both types have been applied to broad geomorphic questions (e.g., controls on drainage density) despite the lack of a firm basis for applying one or the other model type. **Figures 8(a)** and **9(a)** illustrate landscapes driven to an approximate steady-state condition with the DL and TL models, respectively. **Figure 8(a)** was produced from a DL model using $p_d = 1$, $(\rho_b/\rho_s)U = 0.1$ m kyr^{-1}, $\kappa = 1$ m^2 kyr^{-1}, $K = 0.0005$ kyr^{-1}, $c = 0.01$, $\theta_c = 10$ m, rilled hillslopes with $w_h = 0.1\delta$, and a model domain of 250 m × 750 m. **Figure 9(a)** was produced from a TL model using $p_t = 5/3$, $(\rho_b/\rho_s)U = 0.1$ m kyr^{-1}, $\kappa = 1$ m^2 kyr^{-1}, $k = 0.0001$ m$^{2/3}$ kyr^{-1}, $c = 0.01$, $\theta_c = 1$ m, rilled hillslopes with $w_h = 0.1\delta$, and a model domain of 250 m × 750 m. In an approximate steady-state condition, hillslopes in both models have a similar morphology, that is, they are predominantly convex near the divide and transition from convex to concave with increasing distance toward the valley head, as illustrated in the curvature maps in **Figures 8(b)** and **9(b)**.

Figures 8 and **9** also illustrate the DL and TL model landscapes modeled forward in time following a cessation of rock uplift. **Figures 8(c)** and **8(d)** illustrate the topography predicted by the DL model at two time periods (i.e., $t = 1$ and 2 Myr) following the cessation of uplift, whereas **Figures 9(c)** and **9(d)** illustrate the analogous result for the TL case. In the DL case

(Figures 8(c) and 8(d)), topographic decay occurs as a combination of advective slope retreat and diffusive smoothing. Hillslopes in the DL model develop significant basal concavity over time as the topography decays. Concave hillslope bases are commonly associated with deposition, but in this case they develop despite the purely erosional nature of fluvial/slope-wash processes in the model. In the TL case (Figures 9(c) and 9(d)), the slope evolution is broadly similar to that of the DL cases. Valley floors in the TL case, however, undergo autogenetic cycles of aggradation and incision not present in the DL model. In these cycles, valley-floor and sideslope deposition leads to a more distributary flow pattern that, in turn, promotes further aggradation in a positive feedback until the outlet channel fan develops a sufficiently steep slope to trigger reincision and channel narrowing. During the course of the model run illustrated in Figure 9, each valley floor channel undergoes many such cycles of cutting and filling. Despite the presence of these cut-and-fill cycles and the associated distributary channel networks in valley floors of the TL model, the hillslope morphology in both cases is, at any given point in time, qualitatively similar. These results suggest that distributary channel networks and episodically incised valley floors present in non-steady-state TL-dominated landscapes are the primary qualitative differences between landscapes formed with DL versus TL conditions.

2.3.3 Conclusions

Numerical modeling has become an integral component of the study of landscape evolution. This chapter described the principal techniques used to solve some of the most common diffusive and advective partial differential equations that arise in landscape evolution modeling, with a particular emphasis on landforms dominated by hillslope and fluvial processes. Transport-limited and DL models provide type examples of diffusive and advective equations, respectively. Transport-limited models are applicable to hillslope and fluvial systems dominated by colluvial and/or bed-load transport. DL models are applicable to landscapes dominated by suspended-load transport. The chapter also described some steps that are useful for minimizing the grid-resolution dependence of models when multiple process models are combined and channels are not fully resolved in cross section.

References

Ahnert, F., 1977. Some comments on quantitative formulation of geomorphological processes in a theoretical-model. Earth Surface Processes and Landforms 2, 191–201.

Coulthard, T.J., Hicks, D.M., van de Wiel, M.J., 2007. Cellular modelling of river catchments and reaches: advantages, limitations, and prospects. Geomorphology 90, 192–207.

Cox, N.J., 1980. On the relationship between bedrock lowering and regolith thickness. Earth Surface Processes 5, 271–274.

Culling, W.E.H., 1960. Analytical theory of erosion. Journal of Geology 68, 336–344.

Culling, W.E.H., 1963. Soil creep and the development of hillside slopes. Journal of Geology 71, 127–161.

Freeman, G.T., 1991. Calculating catchment area with divergent flow based on a rectangular grid. Computers and Geosciences 17, 413–422.

Furbish, D.J., Fagherazzi, S., 2001. Stability of creeping soil and implications for hillslope evolution. Water Resources Research 37, 2607–2618.

Gabet, E.J., 2000. Gopher bioturbation: field evidence for nonlinear hillslope diffusion. Earth Surface Processes and Landforms 25, 1419–1428.

Hack, J.T., 1957. Studies of longitudinal stream profiles in Virginia and Maryland. U.S. Geological Survey Professional Paper 294-B, 45–97.

Heimsath, A.M., Dietrich, W.E., Nishiizumi, K., Finkel, R.C., 1997. The soil production function and landscape equilibrium. Nature 388, 358–361.

Heimsath, A.M., Dietrich, W.E., Nishiizumi, K., Finkel, R.C., 2001. Stochastic processes of soil production and transport: erosion rates, topographic variation and cosmogenic nuclides in the Oregon Coast Range. Earth Surface Processes and Landforms 26, 531–552.

Heimsath, A.M., Furbish, D.J., Dietrich, W.E., 2005. The illusion of diffusion: field evidence for depth-dependent sediment transport. Geology 33, 949–952.

Howard, A.D., 1994a. Badlands. In: Abrahams, A.D., Parsons, A.J. (Eds.), Geomorphology of Desert Environments. Chapman and Hall, London, pp. 213–242.

Howard, A.D., 1994b. A detachment-limited model of drainage basin evolution. Water Resources Research 30, 2261–2285.

Ijjasz-Vasquez, E.J., Bras, R.L., 1995. Scaling regimes of local slope versus contributing area in digital elevation models. Geomorphology 12, 299–311.

Istanbulluoglu, E., Tarboton, D.G., Pack, R.T., Luce, C., 2003. A sediment transport model for incision of gullies on steep topography. Water Resources Research 38, 4. http://dx.doi.org/10.1029/2002WR001467.

Leopold, L.B., Maddock, T., Jr., 1953. The hydraulic geometry of stream channels and some physiographic implications. U.S. Geological Survey Professional Paper 252, 57 pp.

Moglen, G.E., Bras, R.L., 1995. The effect of spatial heterogeneities on geomorphic expression in a model of basin evolution. Water Resources Research 31, 2613–2623.

Montgeomery, D.R., Dietrich, W.E., 1988. Where do channels begin? Nature 336, 232–234.

O'Callaghan, J.F., Mark, D.M., 1984. The extraction of drainage networks from digital elevation data. Computer Vision, Graphics, and Image Processing 28(3), 323–344.

Pelletier, J.D., 2008. Quantitative Modeling of Earth Surface Processes. Cambridge University Press, Cambridge.

Pelletier, J.D., 2010. Minimizing the grid-resolution dependence of flow-routing algorithms for geomorphic applications. Geomorphology 122, 91–98.

Perron, J.T., Dietrich, W.E., Kirchner, J.W., 2008. Controls on the spacing of first-order valleys. Journal of Geophysical Research 113, F04016. http://dx.doi.org/10.1029/2007JF000977.

Perron, J.T., Kirchner, J.W., Dietrich, W.E., 2009. Formation of evenly-spaced ridges and valleys. Nature 460, 502–505.

Quinn, P.F., Beven, K.J., Chevallier, P., Planchon, O., 1991. The prediction of hillslope flow paths for distributed hydrological modeling using digital terrain models. Hydrological Processes 5, 59–79.

Roering, J.J., 2004. Soil creep and convex-upward velocity profiles: theoretical and experimental investigation of disturbance-driven sediment transport on hillslopes. Earth Surface Processes and Landforms 29, 1597–1612.

Roering, J.J., 2008. How well can hillslope evolution models 'explain' topography? Simulating soil transport and production with high-resolution topographic data. Geological Society of America Bulletin 120, 1248–1262.

Roering, J.J., Kirchner, J.W., Dietrich, W.E., 1999. Evidence for nonlinear, diffusive sediment transport on hillslopes and implications for landscape morphology. Water Resources Research 35, 853–870.

Roering, J.J., Kirchner, J.W., Dietrich, W.E., 2001. Hillslope evolution by nonlinear, slope-dependent transport: steady-state morphology and equilibrium adjustment timescales. Journal of Geophysical Research 106, 16499–16513.

Simpson, G., Schlunegger, F., 2003. Topographic evolution and morphology of surfaces evolving in response to coupled fluvial and hillslope sediment transport. Journal of Geophysical Research 108, 2300. http://dx.doi.org/10.1029/2002JB002162.

Smith, R.E., Quinton, J., Goodrich, D.C., Nearing, M., 2010. Soil-erosion models: where do we really stand? Earth Surface Processes and Landforms 35, 1344–1348.

Smith, T.R., Bretherton, F.P., 1972. Stability and the conservation of mass in drainage basin evolution. Water Resources Research 8, 1506–1529.

Smolarkiewicz, P.K., 1984. A fully multidimensional positive definite advection transport algorithm with small implicit diffusion. Journal of Computational Physics 54, 325–362.

Tarboton, D.G., 1997. A new method for the determination of flow directions and upslope areas in grid Digital Elevation Models. Water Resources Research 33, 309–319.

Tarboton, D.G., Bras, R.L., Rodriguez-Iturbe, I., 1992. A physical basis for drainage density. Geomorphology 5, 59–76.
Tucker, G.E., Bras, R.L., 1998. Hillslope processes, drainage density, and landscape morphology. Water Resources Research 34, 2751–2764.
Wainwright, J., Parsons, A.J., Muller, E.N., Brazier, R.E., Powell, D.M., Fenti, B., 2008a. A transport distance approach to scaling erosion rates: 1. Background and model development. Earth Surface Processes and Landforms 33, 813–826.
Wainwright, J., Parsons, A.J., Muller, E.N., Brazier, R.E., Powell, D.M., Fenti, B., 2008b. A transport distance approach to scaling erosion rates: 1. Sensitivity and evaluation of MAHLERAN. Earth Surface Processes and Landforms 33, 962–984.
Wainwright, J., Parsons, A.J., Muller, E.N., Brazier, R.E., Powell, D.M., Fenti, B., 2008c. A transport distance approach to scaling erosion rates: 1. Background and model development. Earth Surface Processes and Landforms 33, 813–826.
Whipple, K.X., Tucker, G.E., 1999. Dynamics of the stream-power river incision model: implications for the height limits of mountain ranges, landscape response timescales, and research needs. Journal of Geophysical Research 104, 17661–17674.
Wiberg, P.L., Smith, J.D., 1989. A model for calculating bed load transport of sediment. Journal of Hydraulic Engineering, ASCE 115(1), 101–123.
Willgoose, G., 2005. Mathematical modeling of whole landscape evolution. Annual Reviews of Earth and Planetary Sciences 33, 443–459.
Willgoose, G., Bras, R.L., Rodriguez-Iturbe, I., 1991. A coupled channel network growth and hillslope evolution model 1. Theory. Water Resources Research 27, 1671–1684.

Biographical Sketch

Jon Pelletier has a BS degree in physics from the California Institute of Technology and a PhD from Cornell University in geological sciences. He has been a professor in the Geosciences Department at the University of Arizona since 1999. His research aims to combine numerical modeling, remote sensing, and field observations of hillslope, fluvial, aeolian, and glacial geomorphology. He has also worked on surface processes on Mars, climate dynamics, earthquake mechanics, and the dynamics of ecological systems.